Nonadiabatic dynamics in Rydberg gases with random atom positions

Ritesh Pant,[1] Rajat Agrawal,[2] Sebastian Wüster,[1] and Jan-Michael Rost[2]
[1]*Department of Physics, Indian Institute of Science Education and Research, Bhopal, Madhya Pradesh 462 066, India*
[2]*Max Planck Institute for the Physics of Complex Systems, Nöthnitzer Strasse 38, 01187 Dresden, Germany*

(Received 27 June 2021; accepted 3 November 2021; published 2 December 2021)

Assemblies of highly excited Rydberg atoms in an ultracold gas can be set into motion by a combination of van der Waals and resonant dipole-dipole interactions. Thereby, the collective electronic Rydberg state might change due to nonadiabatic transitions, in particular if the configuration encounters a conical intersection. For the experimentally most accessible scenario, in which the Rydberg atoms are initially randomly excited in a three-dimensional bulk gas under blockade conditions, we numerically show that nonadiabatic transitions can be common when starting from the most energetic repulsive Born-Oppenheimer surface. We outline how this state can be selectively excited using a microwave resonance, and demonstrate a regime where almost all collisional ionization of Rydberg atoms can be traced back to a prior nonadiabatic transition. Since Rydberg ionization is relatively straightforward to detect, the excitation and measurement scheme considered here renders nonadiabatic effects in Rydberg motion easier to demonstrate experimentally than in scenarios considered previously.

DOI: 10.1103/PhysRevA.104.063303

I. INTRODUCTION

Collections of a small number of highly excited Rydberg atoms in a cold gas or even BEC are nowadays routinely created in laboratories. The motion of these atoms can often be neglected on the timescale of experiments, justifying the so-called frozen gas approximation. However, under generic circumstances, namely, for lighter atoms and initial close proximity, they are easily set into motion on timescales of interest by nonresonant van der Waals (vdW) or resonant dipole-dipole (DD) interactions [1–5]. The motion of a randomly distributed assembly of Rydberg atoms in three dimensions (3D) has been studied in experiments so far, mainly due to interactions involving a single Rydberg state [6–10], permanent dipoles [11,12], or transition dipole-dipole interactions of two Rydberg atoms [13,14]. More complex dynamics arises when transition dipole-dipole interactions involve a large number of atoms, giving rise to collective exciton states with a delocalized excitation [15,16]. While a single Rydberg dimer possesses only strongly repulsive or attractive electronic states, the multiatom system has states in which the resonant DD contribution vanishes for the closest pair of atoms. If the remaining repulsive van der Waals interactions are too weak to counteract kinetic energy initially gained from dipole-dipole repulsion, atoms paired in these states can collisionally ionize if they hit a neighboring Rydberg atom.

An additional feature of collective dipole-dipole interactions are conical intersections (CIs) between adjacent electronic states of the multiatom Rydberg assembly [17]. Near a conical intersection, nonadiabatic transitions necessarily become likely. These transitions play a key role in many quantum chemical processes [18], such as photochemistry of vision [19] or DNA protection from UV radiation damage [20]. While computational methods can nowadays provide an impressive level of detail for multidimensional nuclear wave functions of molecules [21,22], such detail is hard to record when interrogating molecules experimentally. More detail may be accessible when studying the dynamics around conical intersections with cold atoms or molecules [23–26], Rydberg atoms [16,17], or ions [27].

Towards the long-term goal to quantum simulate the processes above with ultracold Rydberg atoms, we study one of the simplest scenarios that can experimentally give rise to dynamics involving CIs with Rydberg atoms. Even if these are initialized in a state in which the nearest atoms should repel, nonadiabatic transitions or passages through CIs can transfer the electronic state to a nonrepelling one. After that transfer, Rydberg atoms can ionize. We demonstrate that for a suitable choice of parameters, most ionization events can be traced back to at least one nonadiabatic transition, implying conversely that ionization is an easily accessible experimental signature for a nonadiabatic transition. In comparison to earlier proposals to investigate conical intersections in Rydberg systems [17,28–30], the scenario discussed in this article lifts the challenges of constraining the motion of atoms through trapping, tightly localizing the Rydberg excitation and high-resolution Rydberg position measurements.

This article is organized as follows: In Sec. II, we introduce the model for collective dipole-dipole interactions of Rydberg atoms, the quantum-classical propagation scheme employed, and our phenomenological model of the excitation sequence. In Sec. III, we explore nonadiabatic dynamics with individual trajectories of the classical motion of Rydberg atoms, to clearly connect ionization with nonadiabatic transitions. Finally, in Sec. IV, we portray the dynamics in the trajectory-averaged energy spectrum of the system.

II. DIPOLE-DIPOLE INTERACTIONS IN 3D RYDBERG GASES

We consider an assembly of N lithium Rydberg atoms, each with mass $M \approx 11\,000$ a.u. and principal quantum number ν. All atoms can move freely in 3D, with their collective positions described by the $3N$-component vector $\mathbf{R} = (\mathbf{r}_1, \ldots, \mathbf{r}_N)^T$, where $\mathbf{r}_k$ is the position of atom number k. We are interested in the joint effect of DD and vdW interactions. Hence, besides constraining ν, we consider angular momentum states $|s(l=0)\rangle$ and $|p(l=1), m\rangle$. For scenarios with only a single Rydberg atom in a $|p\rangle$ state, the collective electronic basis can then be written as $\{|\pi_n(m)\rangle\}$, where

$$|\pi_n(m)\rangle = |s \ldots (p, m) \ldots s\rangle \tag{1}$$

represents the state where the nth atom carries the p excitation with magnetic quantum number m, and all other atoms are in the $|s\rangle$ state. We thus neglect spin-orbit coupling, a reasonable approximation for light atoms such as lithium.

The resulting Hamiltonian for our system reads

$$\hat{H} = -\frac{\hbar^2}{2M}\nabla^2_{\mathbf{R}} + \hat{H}_{el}(\mathbf{R}), \tag{2}$$

where the first term accounts for the kinetic energy of the Rydberg atoms and $\hat{H}_{el}(\mathbf{R}) = \hat{H}_{dd}(\mathbf{R}) + \hat{H}_{vdw}(\mathbf{R})$, with the resonant dipole-dipole interactions

$$\hat{H}_{dd}(\mathbf{R}) = \sum_{\substack{n,n'=1 \\ m,m'}}^{N} V^{(dd)}_{mm'}(\mathbf{R}_{n,n'})|\pi_n(m)\rangle\langle\pi_{n'}(m')|. \tag{3}$$

Here, $V^{(dd)}_{mm'}(\mathbf{R}_{n,n'})$ are the matrix elements for the dipole-dipole interactions between atoms n and n'. They depend on $\mathbf{R}_{nn'} = \mathbf{r}_n - \mathbf{r}_{n'}$ and are explicitly given by [5]

$$V^{(dd)}_{mm'}(\mathbf{R}_{nn'}) = -\sqrt{\frac{8\pi}{3}}\frac{\mu^2}{4\pi\epsilon_0 R^3_{nn'}}(-1)^{m'} \times \begin{pmatrix} 1 & 1 & 2 \\ m & -m' & m'-m \end{pmatrix} Y_{2,m'-m}(\theta_{nn'}, \phi_{nn'}), \tag{4}$$

where μ is the transition dipole moment of the Rydberg atoms associated with the transition between the state $|s\rangle$ and state $|p\rangle$, $R_{nn'} = |\mathbf{R}_{nn'}|$, $\theta_{nn'}$ and $\phi_{nn'}$ are the polar angle and azimuthal angle of the interatomic distance vector, respectively, as shown in Fig. 1, and the six numbers in the parentheses denote the Wigner $3-j$ symbol. Note that resonant dipole-dipole interactions are, in general, anisotropic due to the dependence on θ and ϕ in (4) and mix the different azimuthal sublevels m. The anisotropy and the azimuthal state mixing could be suppressed using Zeeman shifts [29]; however, here we are interested in the pristine scenario.

The term $\hat{H}_{vdw}(\mathbf{R})$ in $\hat{H}_{el}(\mathbf{R})$ pertains to the nonresonant van der Waals interaction,

$$\hat{H}_{vdw}(\mathbf{R}) = -\frac{1}{2}\sum_{n,n'=1}^{N}\frac{C_6}{R^6_{nn'}}\mathbb{I}, \tag{5}$$

where $\mathbb{I}$ is the unit operator in the electronic space and C_6 is the dispersion coefficient which characterizes the strength of the van der Waals interactions dependent on the principal quantum number ν. The van der Waals interactions only become relevant at small interatomic separations since they fall off as $1/R^6_{nn'}$. At large separation, the dipole-dipole interaction given in Eq. (4) dominates over the van der Waals interaction due to the $1/R^3_{nn'}$ dependence on the distance of the former. Throughout this article, we shall assume atoms in $\nu = 80$ and hence $C_6 = -1.7 \times 10^{22}$ a.u. from [31] and $\mu = 4096$ a.u. in (4).

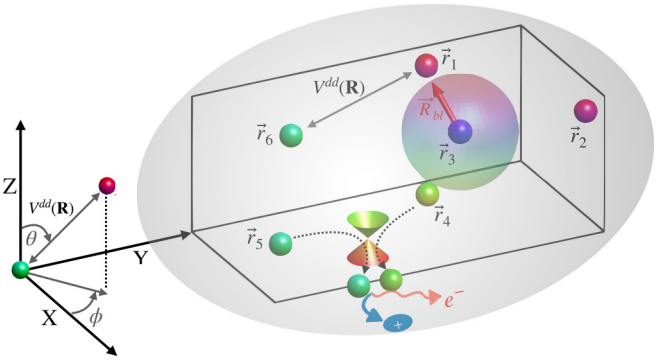

FIG. 1. Sketch of a randomly distributed assembly of Rydberg atoms (spherical balls) in a 3D bulk gas (gray shade) at locations $\mathbf{r}_1, \ldots, \mathbf{r}_6$. R_{bl} is the blockade radius shown by the smaller transparent sphere, representing the initial minimal distance. After passing through a conical intersection (double cones) or region of strong nonadiabatic coupling, atomic repulsion can be overcome and the collision of two Rydberg atoms (here, 4 and 5) results in ionization.

A full-fledged quantum mechanical simulation of the time-dependent Schrödinger equation (TDSE) for the Hamiltonian defined in Eq. (2) is computationally not possible for useful atom numbers N. Hence we employ Tully's surface hopping algorithm [32], which was extensively benchmarked for scenarios such as the present one by direct comparison with Schrödinger's equation in smaller systems, and showed excellent performance [28,33,34]. This is because the repelling assembly of Rydberg atoms never revisits the same many-body coordinate twice, and hence the phases of the nuclear wave function that are not captured by the method cannot become relevant. Tully's algorithm is a quantum-classical method in which the motion of the Rydberg atoms is simulated classically using Newton's equation of motion,

$$M\frac{\partial^2\mathbf{R}}{\partial t^2} = -\nabla_{\mathbf{R}}U_s[\mathbf{R}(t)], \tag{6}$$

where s is the index of the Born-Oppenheimer (BO) surface $U_{k=s}[\mathbf{R}(t)]$ on which the Rydberg system is presently evolving. The surfaces follow from the eigenvalue equation

$$\hat{H}_{el}(\mathbf{R})|\varphi_k(\mathbf{R})\rangle = U_k(\mathbf{R})|\varphi_k(\mathbf{R})\rangle, \tag{7}$$

where we order eigenstates according to increasing energy with increasing index k.

In contrast to the positions, the electronic state of the Rydberg assembly $|\psi(t)\rangle = \sum_{nm} c_{nm}(t)|\pi_n(m)\rangle$ is evolved quantum mechanically with Schrödinger's equation,

$$i\hbar\frac{\partial}{\partial t}c_{nm}(t) = \sum_{n'm'}\langle\pi_n(m)|\hat{H}_{el}(\mathbf{R})|\pi_{n'}(m')\rangle c_{n'm'}(t). \tag{8}$$

It is instructive to also express (8) in the adiabatic basis $|\psi(t)\rangle = \sum_k \tilde{c}_k(t)|\varphi_k(\mathbf{R})\rangle$ formed by the solutions of (7). In

terms of this basis, the TDSE reads

$$i\hbar\frac{\partial}{\partial t}\tilde{c}_k(t) = U_k[\mathbf{R}(t)]\tilde{c}_k(t) - i\hbar\sum_l d_{kl}(t)\tilde{c}_l(t), \tag{9}$$

with nonadiabatic coupling vectors

$$d_{kl} \approx -\frac{1}{M}\langle\varphi_k(\mathbf{R})|\nabla_{\mathbf{R}}|\varphi_l(\mathbf{R})\rangle\cdot\frac{\partial\mathbf{R}}{\partial t}. \tag{10}$$

The latter couple the different BO surfaces, which is implemented into the motional dynamics (6) of Tully's method by allowing stochastic jumps of the index $s \to s'$ with a probability set by $d_{ss'}$. The adiabatic and the diabatic coefficients are connected by the relation $\tilde{c}_k = \sum_{nm} c_{nm}\langle\varphi_k(\mathbf{R})|\pi_n(m)\rangle$. Our simulations employ Tully's method with Eq. (8) coupled to Eq. (6), but one can refer to Eq. (9) for understanding nonadiabatic transitions.

Excitation process and blockade

The initial excitation of Rydberg atoms to states involving $|\pi_n(m)\rangle$ is a two-step process. First, within a bulk ultracold gas, ground-state atoms are excited to the Rydberg state $|s\rangle$, typically using a two-photon excitation [35]. Due to the strong vdW interactions between Rydberg atoms in the state $|s\rangle$, this step is affected by the dipole blockade, which prohibits the excitation of more than one atom within a sphere with blockade radius R_{bl}. We estimate R_{bl} as the distance at which the strength of the van der Waals interactions becomes equal to the broadened linewidth of a laser with Rabi frequency Ω_{las} [36,37], resulting in

$$R_{bl} = \left(\frac{|C_6|}{\Omega_{las}}\right)^{1/6}. \tag{11}$$

For our simulation, we assume $\Omega_{las}/(2\pi) \approx 60$ MHz, which for $\nu = 80$ results in $R_{bl} = 5.9\ \mu$m. The bulk excitation and blockade are then phenomenologically taken into account by drawing random positions from a sphere of radius $R = 4R_{bl}$ in 3D, and discarding those with $R_{nm} < R_{bl}$ for any pair of Rydberg atoms. A more sophisticated approach could model the excitation process using classical rate equations [38]. The radius of the sphere is practically motivated to ensure that the atoms are not crammed too closely initially, and not too far spaced to miss colliding with each other after the initial acceleration. After completing this first step of the process, we have an assembly of N Rydberg atoms all in the state $|s\rangle$ (hence in a many-body state $|s..s..\rangle$) at random positions $\mathbf{R}_{\rm ini}$ consistent with the excitation blockade.

In the second step, we induce a p excitation to enable resonant dipole-dipole interactions with a near resonant microwave pulse to $|\pi_n(m)\rangle$, linearly polarized along the quantization axis. The corresponding Hamiltonian reads

$$\hat{H}_{mw} = \sum_n \frac{\Omega}{2}[|\pi_n(0)\rangle\langle s| + \text{c.c.}] - \sum_n \Delta|\pi_n(0)\rangle\langle\pi_n(0)|, \tag{12}$$

where Ω is the Rabi frequency of the microwave and Δ its detuning from the bare sp transition. By this detuning, it is possible to excite a chosen exciton state $|\varphi_k\rangle$ in (7) based on the knowledge of the initial distribution of the position of the atoms and thus the mean exciton energies, while avoiding more than one p excitation [34]. Even if, for randomly placed atoms such as here, we encounter an accidental two-photon resonance of an exciton state with two p excitations [39], the intermediate singly excited state will be off resonant, slowing the double excitation down such that it is negligible for short microwave pulses.

In practice, after atoms have been excited to Rydberg s states at random initial positions $\mathbf{R}_{\rm ini}$ as discussed above, the relative excitation probability $P_r(k)$ of state $|\varphi_k(\mathbf{R}_{\rm ini})\rangle$ will depend on two factors: (i) The transition matrix element between $|s..s..\rangle$ and $|\varphi_k(\mathbf{R}_{\rm ini})\rangle$, which depends on the microwave polarization direction, and (ii) the microwave frequency (detuning). We incorporate both effects phenomenologically in Tully's algorithm by randomly starting the simulation in exciton state k with relative probability

$$P_r(k) = \mathcal{N}e^{-\frac{(U_k-\Delta)^2}{2\sigma_U^2}}\tilde{P}_r(k), \tag{13}$$

where U_k are the exciton energies defined in Eq. (7), Δ is the microwave detuning, σ_U is the microwave linewidth, and $\tilde{P}_r(k)$ is a polarization-dependent factor, discussed in the Appendix, that takes into account the matrix element. The normalization factor $\mathcal{N}$ ensures $\sum_k P_r(k) = 1$, and trajectories with $|U_k - \Delta| > 2\sigma_U$ for all k are discarded. Importantly, $P_r(k)$ contains a twofold dependence on the initial positions of the Rydberg atoms after they have been excited to $|s..s..\rangle$: through the exciton energies U_k and the interplay of microwave polarization and locations encoded in $\tilde{P}_r(k)$.

III. NONADIABATIC DYNAMICS FROM RANDOM INITIAL POSITIONS

We are now in a position to study the motional dynamics of $N = 6$ Rydberg atoms, starting from initial locations $\mathbf{R}_{\rm ini}$ as discussed in Sec. II to explore how motion depends on the choice of the initially excited repulsive BO surface k defined in Eq. (7). Such a configuration is illustrated in Fig. 2(a), where the colored spheres represent the initial positions of the Rydberg atoms. A single realization of the time evolution of atomic positions when the system is prepared in the highest-energy repulsive state (i.e., $k = 3N = 18$) is shown by the solid lines in 3D with the projection of trajectories onto the XY plane indicated by the dashed lines. Figure 2(b) shows the time evolution of all the electronic energy surfaces $U_k[\mathbf{R}(t)]$ on the left y axis, together with the minimum distance $d_{\rm min} = \min_{nm} R_{nm}$ between the atoms, shown as a thick gray line using the right y axis. We have selected a trajectory without nonadiabatic transition, staying on the highest-energy repulsive surface. Even when the initially accelerated atoms now encounter new collision partners, which happens around $t \approx 5\ \mu$s and causes $d_{\rm min}$ to exhibit a local minimum, the repulsion prevents a close encounter with ionization. A qualitatively different trajectory is shown in Figs. 2(c) and 2(d), where the system undergoes a sequence of nonadiabatic transitions from the highest-energy repulsive surface to the surface with index $k = 15$, as shown by the adiabatic populations in Fig. 2(c) and the red dashed lines in Fig. 2(d). The transitions are due to significant nonadiabatic coupling terms d_{kl} in Eq. (9), usually when adjacent BO surfaces approach each other closely in energy. We find that on the surface $k = 15$, atoms no longer

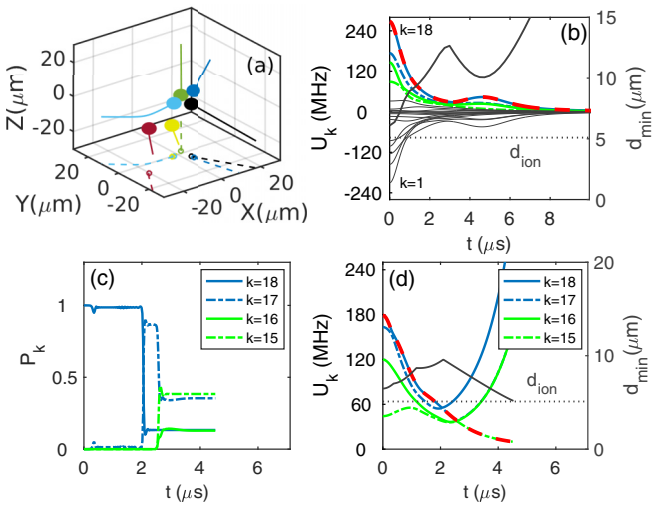

FIG. 2. Electronic and motional Rydberg dynamics for the system prepared in the highest-energy electronic state. (a),(b) Trajectory without nonadiabatic transition. (c),(d) Trajectory with nonadiabatic transition. (a) Initial configuration (colored balls) and trajectories (solid lines) of the atomic positions $\mathbf{r}_k(t)$. Colored circles and dashed lines show the projection of initial positions and trajectories onto the XY plane. (b) Time evolution of potential energies $U_k[\mathbf{R}(t)]$ and the minimum distance $d_{\min}$ between atoms (thick gray line, right axis) without nonadiabatic coupling. d_{ion} is the ionization distance defined in Eq. (14) (gray dotted line). (c) Adiabatic populations on the four highest-energy repulsive surfaces, showing nonadiabatic dynamics. (d) Time evolution of potential energies $U_k[\mathbf{R}(t)]$ similar to (b). The presently propagated surface s in Eq. (6) is shown as a red dashed line, and the three highest potential energies and d_{ion} are color coded as in (c).

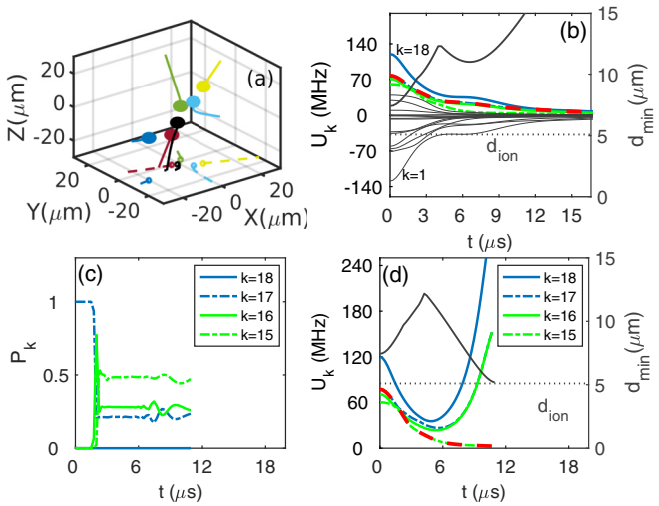

FIG. 3. The same as Fig. 2, but starting from the the second most energetic electronic eigenstate $k = 17$, instead of the highest energy one $k = 18$.

repel, and hence the minimal distance $d_{\min}$ decreases continuously after $\approx 2\ \mu$s when two Rydberg atoms encounter one another. If that happens, they would typically ionize, which we phenomenologically model by declaring atoms collisionally ionized when they come closer than an ionization distance d_{ion} where the simulation is aborted, as shown in Figs. 2(c) and 2(d). We take d_{ion} as the distance below which the Rydberg energy spectra become dense when taking all electronic states into account. For such close distances, our effective state model based solely on $|s\rangle$ and $|p\rangle$ would break down. A complete treatment of ionization would thus require the full electronic space state, which would go substantially beyond the scope of the present paper. Hence we use a rough estimate of d_{ion}, which is provided by the formula [16]

$$d_{ion}(n) = 2\left[\frac{\mu^2 n^3}{\Delta E_{pd}(n)}\right]^{1/3}, \tag{14}$$

where ΔE_{pd} is the energy difference between $|p\rangle$ and the nearest Rydberg state not included in the model, $|d(l=2)\rangle$. For the example shown in Fig. 2, the nonadiabatic transition therefore ultimately leads to ionization of the Rydberg atoms after $t = 4\ \mu$s, much earlier than the lifetime $\tau \approx 50\ \mu$s of our six-atoms system [16,40].

Next, we show that qualitatively similar dynamics can be found when the Rydberg assembly is initialized on the next few less energetic energy surfaces, starting in Fig. 3 from $k = 17$. The figure illustrates the atomic dynamics up to the ionization time, in Fig. 3(a) together with the time evolution of the electronic energy eigenstates and in Figs. 3(b) and 3(d) with the minimum distance between atoms. We see in Figs. 3(c) and 3(d) that due to the nonadiabatic coupling, the system can quickly jump from surface $k = 17$ to $k = 15$, where it is later ionized. To underscore the need for nonadiabatic transitions, we also show in Fig. 3(b) the time evolution of eigenstates and minimal distance when nonadiabatic jumps of the surface index s in Eq. (6) are disabled, but using the same initial configuration as in Figs. 3(c) and 3(d). As a consequence, the system remains on the surface $k = 17$, maintaining repulsive dynamics without ionization. The scenario is qualitatively similar when starting on the surface $k = 16$. In all cases, the first surface for which repulsion is lost and the Rydberg atoms can ionize is $k = 15$ for $N = 6$. Consequently, we find that when starting on $k = 15$, ionization is possible even without a prior nonadiabatic transition. This is not the case for any of the higher surfaces. These characterizations of surfaces are for six Rydberg atoms. If we vary the number of atoms, we find that for N atoms, the ionization takes place from the $3(N-1)$th energy surface. We can understand this by inspection of a dimer, which has three repulsive surfaces due to the availability of three azimuthal quantum numbers. This property is inherited by the many-atom system since the collision properties are only governed by the closest proximity pair.

Our inspection of single trajectories starting on the three highest-energy surfaces with indices $k = 16, 17, 18$ has revealed that ionization of Rydberg atoms must be preceded by at least one nonadiabatic transition. Therefore, the observation of collisional ionization of Rydberg atoms after initializing the system repulsively can be used as a signature of nonadiabatic transitions in the experiment.

IV. AVERAGED DYNAMICS

The single trajectory simulations in Sec. III from selected electronic states provide a more detailed picture of the dynamics, but they would not be individually experimentally

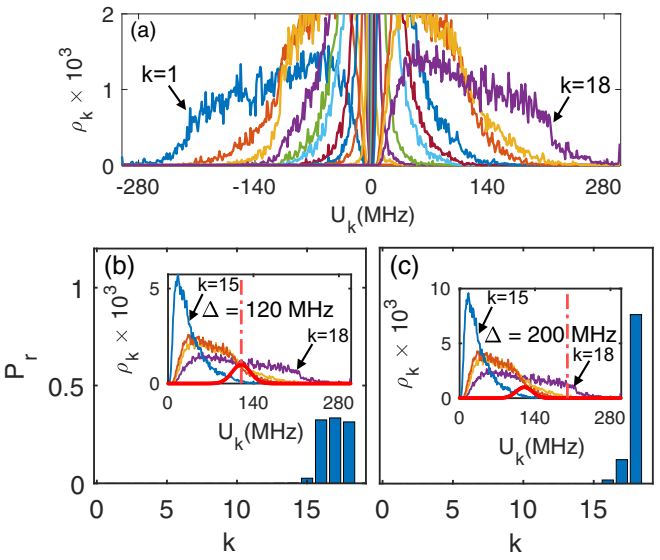

FIG. 4. (a) Probability distribution ρ_k of energies U_k, $1 \leqslant k \leqslant 18$, for 5000 random configurations ($\mathbf{R}$) of atoms. We show a zoom on the high-energy flank in (b) and (c), together with a certain microwave line profile P_r (thick red line) with detuning (b) $\Delta = 120$ and (c) $\Delta = 200$ MHz, respectively. The inset shows the resultant surface index distribution after excitation, according to Eq. (13).

accessible. Instead, one has to average over many repetitions of an experiment and address exciton states through the microwave detuning, corresponding to multitrajectory averages with random initial electronic states according to (13). We present these averaged simulations in this section.

In the proposed experiment with random Rydberg excitation location in a bulk gas, initializing a specific exciton state k will pose practical challenges. The most straightforward approach would be detuning a microwave, as discussed in Sec. II, such that it is resonant with that state: $\Delta = U_k$. However, the exciton energies U_k depend on all Rydberg positions $\mathbf{R}_{\text{ini}}$, which are random subject to constraints by the blockade. As an initial step to address this challenge, we show the histogram of initial exciton energies for those random positions in Fig. 4. While the energy distribution of energetically neighboring excitons usually overlaps, we can see that the tails contain energy regions where only the highest-energy surface is present. Choosing a detuning in that region, e.g., $\Delta = 200$ MHz and narrow linewidth $\sigma_U = 15.0$ MHz, we can achieve excitation of the Rydberg assembly almost entirely on the highest-energy surface, as shown in Fig. 4(c). For realizations of positions in which the atoms are too far apart to provide an exciton with these high energies, no excitation would happen for this detuning in an experiment. We model only the cases where excitation of a $|p\rangle$ state is successful. For the distribution of excited surfaces, we phenomenologically model the microwave excitation probability (13) with more details in the Appendix. Lowering the detuning to $\Delta = 120$ MHz and $\sigma_U = 15.0$ MHz allows a tuning of the distribution of surfaces k, with almost equal contributions of the three highest ones, $k = 16, 17, 18$.

We now present multitrajectory surface-hopping simulations starting from random initial state distributions as shown in Fig. 4, using $\Delta = 200$ MHz such that the probability of

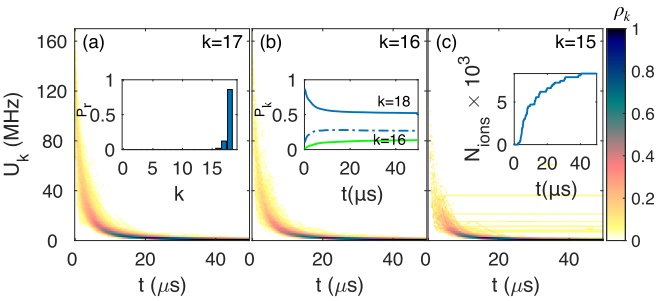

FIG. 5. Mean time-resolved potential energy density on the (a) second, (b) third, and (c) fourth most energetic BO surface, starting with the microwave detuned to $\Delta = 200$ MHz so that the system most likely begins on the first surface. To emphasize low-density features, we plot the square root of the energy densities and adjust the color bar range. The insets show (a) the relative initial excitation probability of each surface, (b) adiabatic populations, and (c) the mean number of ions per trajectory as a function of time.

excitation onto the highest-energy repulsive surface is 90%; see inset of Fig. 5(a). The figure shows the time and surface resolved potential energy density $\rho_s(t)$, which we construct by binning the potential energy $U_s(t)$ of the currently propagated BO surface $s(t)$. To this end, the energy axis is divided into equidistant bins, to then obtain the mean number of trajectories with $U_s(t)$ within a given bin at each time; see also [30].

We see in Fig. 5 that from the highest-energy surface, the system jumps nonadiabatically to lower-energy surfaces and then ultimately can be ionized after reaching the surface with index $k = 15$. Since ionization is implemented by stopping the time evolution and sampling constant quantities thereafter, it shows up in these histograms as (unphysical) horizontal stripes, which are to be taken simply as a pointer towards the ionization event (where the stripes intersect the bulk distribution). If the detuning is reduced to $\Delta = 120$ MHz with linewidth $\sigma_U = 15.0$ MHz, one significantly excites three of the highest-energy surfaces, as shown in Fig. 4(b). This relative transition probability is again shown in the inset of Fig. 6(a). Starting from such an initial state, Fig. 6 shows the evolution of time-resolved potential energy density for the three most strongly participating surfaces, similarly to Fig. 5. Since fewer nonadiabatic transitions are required on average to reach the ionizing surface, this scenario exhibits an about three-times-higher ionization signal than the one of Fig. 5.

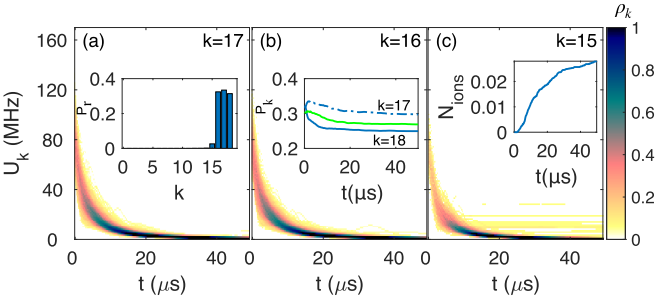

FIG. 6. Mean time-resolved potential energy density similar to Fig. 5, but for the microwave detuning of $\Delta = 120$ MHz, such that more surfaces are populated initially.

The spectra, as shown in Figs. 5 and 6, are experimentally accessible through microwave spectroscopy, as in [9].

Overall we have shown that for both these microwave detunings, ionization of the Rydberg atoms is strongly linked to nonadiabatic transitions since the system will be initialized solely on surfaces on which ionization does not occur directly, as shown in Sec. III. We also demonstrated that on the high-energy tails of the initial energy distribution, a reasonable control over the initial exciton state is possible through the microwave detuning. The control over the initial state translates into control over the ionization probability.

The rate of ionization for the simulations presented here remains relatively low, which is an artifact of our restriction to just $N = 6$ atoms to keep simulations tractable. For only six atoms, it is relatively unlikely that a pair of atoms initially repel, the system then undergoes nonadiabatic transitions to leave the repelling surfaces, and an atom subsequently still encounters a new collision partner on its outwards journey in order to ionize. The situation would be very different in an experiment, where a much larger number of Rydberg atoms can be easily excited. If the initially repelling atoms are surrounded in all directions by a larger number of Rydberg atoms, it is reasonable to expect that the ionization probability after a nonadiabatic transition could approach unity.

Along the same lines, while the simulations presented here are for lithium atoms, the equivalent simulations with rubidium atoms showed qualitatively similar behavior, but even smaller ionization probabilities within the lifetime of the atoms due to their larger inertia. This could likely be overcome by a larger number of atoms in experiments, such that we expect our results to qualitatively also pertain to rubidium assemblies.

V. CONCLUSIONS

We have modeled the joint electronic and motional dynamics of an assembly of few ($N = 6$) Rydberg excitations that are created at random 3D positions in an ultracold gas. Atoms subsequently move according to resonant dipole-dipole interactions. With a simple phenomenological model for microwave excitation with a fixed detuning, we have shown that experiments can selectively initialize this motional dynamics in dipole-dipole exciton eigenstates that have entirely repulsive character. We have modeled the motion of the Rydberg assembly with a quantum classical surface-hopping algorithm, which permits nonadiabatic transitions between exciton states.

These simulations reveal frequent nonadiabatic transitions for the parameters selected, rendering it likely that the group of Rydberg atoms reaches a Born-Oppenheimer surface that is no longer repulsive and therefore permits collisional ionization of Rydberg atoms. This causal chain of events turns an ion count into an experimentally accessible flag for nonadiabatic transitions.

Earlier simulations of nonadiabatic dynamics near conical intersections in Rydberg systems assumed trapped Rydberg atoms [17,28,29] or tightly localized excitation beams [30], and require high-resolution Rydberg position measurements for the observation of the results. While possible with a dedicated apparatus [10,12,41,42], these requirements pose a challenge to most ultracold Rydberg experiments. In contrast, the results presented here should be observable using routinely applied random Rydberg excitation in a thermal gas and interrogation via ion counting.

ACKNOWLEDGMENTS

It is a pleasure to thank Kaustav Mukherjee for helpful comments and Karsten Leonhardt for contributions to the codes used. We also thank the Max-Planck Gesellschaft for financial support under the MPG-IISER partner group program. R.P. is grateful to the Council of Scientific and Industrial Research (CSIR), India, for a Shyama Prasad Mukherjee (SPM) fellowship for pursuing the Ph.D. (File No. SPM-07/1020(0304)/2019-EMR-I).

APPENDIX: MICROWAVE TRANSITIONS

The exciton states defined in (7) can be expressed explicitly in the basis (1) as

$$|\varphi_k\rangle = \sum_{m,n} f_{nm}^{(k)} |\pi_n(m)\rangle, \tag{A1}$$

where $f_{nm}^{(k)} = \langle\varphi_k|\pi_n(m)\rangle$ are the component amplitudes in the basis state $|\pi_n(m)\rangle$ for the system eigenstate $|\varphi_k\rangle$. With (A1), the transition probability P_k from the $|s..s..\rangle$ state to the exciton state Eq. (A1), using Eq. (12), is proportional to

$$P_k \propto |\langle\varphi_k|\hat{H}_{mw}|s..s..\rangle|^2 \propto \left[\sum_n f_{n0}^{(k)}\right]^* \left[\sum_n f_{n0}^{(k)}\right]. \tag{A2}$$

We are not interested in absolute probabilities for the simulation since we only want to model trajectories where *some* exciton state has been excited, but (A2) is sufficient to infer the relative transition probability $\tilde{P}_r(k)$ onto the BO surface k as

$$\tilde{P}_r(k) = \frac{P_k}{\sum_k P_k}. \tag{A3}$$

Using Eq. (A3), the relative transition probability for different microwave detunings Δ is shown in Figs. 4(b) and 4(c). For simulations in Figs. 5 and 6, we remove trajectories for which all exciton energies are far from the microwave resonance, $|U_k - \Delta| > 2\sigma_U \ \forall k$, since when using an absolute excitation probability these cases would simply not show any excitation of Rydberg p states.

[1] S. D. Gensemer and P. L. Gould, Phys. Rev. Lett. **80**, 936 (1998).

[2] W. Li, P. J. Tanner, and T. F. Gallagher, Phys. Rev. Lett. **94**, 173001 (2005).

[3] A. Fioretti, D. Comparat, C. Drag, T. F. Gallagher, and P. Pillet, Phys. Rev. Lett. **82**, 1839 (1999).

[4] K. R. Overstreet, A. Schwettmann, J. Tallant, and J. P. Shaffer, Phys. Rev. A **76**, 011403(R) (2007).

[5] F. Robicheaux, J. V. Hernandez, T. Topcu, and L. D. Noordam, Phys. Rev. A **70**, 042703 (2004).

[6] M. Viteau, A. Chotia, D. Comparat, D. A. Tate, T. F. Gallagher, and P. Pillet, Phys. Rev. A **78**, 040704(R) (2008).

[7] T. Amthor, M. Reetz-Lamour, S. Westermann, J. Denskat, and M. Weidemüller, Phys. Rev. Lett. **98**, 023004 (2007).

[8] T. Amthor, M. Reetz-Lamour, C. Giese, and M. Weidemüller, Phys. Rev. A **76**, 054702 (2007).

[9] R. C. Teixeira, C. Hermann-Avigliano, T. L. Nguyen, T. Cantat-Moltrecht, J. M. Raimond, S. Haroche, S. Gleyzes, and M. Brune, Phys. Rev. Lett. **115**, 013001 (2015).

[10] N. Thaicharoen, A. Schwarzkopf, and G. Raithel, Phys. Rev. A **92**, 040701(R) (2015).

[11] L. F. Gonçalves, N. Thaicharoen, and G. Raithel, J. Phys. B: At. Mol. Opt. Phys. **49**, 154005 (2016).

[12] N. Thaicharoen, L. F. Gonçalves, and G. Raithel, Phys. Rev. Lett. **116**, 213002 (2016).

[13] H. Park, P. J. Tanner, B. J. Claessens, E. S. Shuman, and T. F. Gallagher, Phys. Rev. A **84**, 022704 (2011).

[14] H. Park, E. S. Shuman, and T. F. Gallagher, Phys. Rev. A **84**, 052708 (2011).

[15] C. Ates, A. Eisfeld, and J. M. Rost, New J. Phys. **10**, 045030 (2008).

[16] S. Wüster and J. M. Rost, J. Phys. B: At. Mol. Opt. Phys. **51**, 032001 (2018).

[17] S. Wüster, A. Eisfeld, and J. M. Rost, Phys. Rev. Lett. **106**, 153002 (2011).

[18] M. Dantus and A. Zewail, *Introduction: Femtochemistry* (ACS Publications, 2004).

[19] S. Hahn and G. Stock, J. Phys. Chem. B **104**, 1146 (2000).

[20] S. Perun, A. L. Sobolewski, and W. Domcke, J. Am. Chem. Soc. **127**, 6257 (2005).

[21] I. Burghardt, K. Giri, and G. A. Worth, J. Chem. Phys. **129**, 174104 (2008).

[22] G. A. Worth, H. D. Meyer, H. Köppel, L. S. Cederbaum, and I. Burghardt, Intl. Rev. Phys. Chem. **27**, 569 (2008).

[23] A. O. G. Wallis, S. A. Gardiner, and J. M. Hutson, Phys. Rev. Lett. **103**, 083201 (2009).

[24] N. Moiseyev, M. Šindelka, and L. S. Cederbaum, J. Phys. B: At. Mol. Opt. Phys. **41**, 221001 (2008).

[25] S. L. Zhu, B. Wang, and L.-M. Duan, Phys. Rev. Lett. **98**, 260402 (2007).

[26] J. Larson and E. Sjöqvist, Phys. Rev. A **79**, 043627 (2009).

[27] F. M. Gambetta, C. Zhang, M. Hennrich, I. Lesanovsky, and W. Li, Phys. Rev. Lett. **126**, 233404 (2021).

[28] K. Leonhardt, S. Wüster, and J. M. Rost, Phys. Rev. Lett. **113**, 223001 (2014).

[29] K. Leonhardt, S. Wüster, and J. M. Rost, Phys. Rev. A **93**, 022708 (2016).

[30] K. Leonhardt, S. Wüster, and J. M. Rost, J. Phys. B: At. Mol. Opt. Phys. **50**, 054001 (2017).

[31] K. Singer, J. Stanojevic, M. Weidemüller, and R. Côté, J. Phys. B: At. Mol. Opt. Phys. **38**, S295 (2005).

[32] J. C. Tully, J. Chem. Phys. **93**, 1061 (1990).

[33] S. Wüster, C. Ates, A. Eisfeld, and J. M. Rost, Phys. Rev. Lett. **105**, 053004 (2010).

[34] S. Möbius, S. Wüster, C. Ates, A. Eisfeld, and J. Rost, J. Phys. B: At. Mol. Opt. Phys. **44**, 184011 (2011).

[35] R. Löw, H. Weimer, J. Nipper, J. B. Balewski, B. Butscher, H. P. Büchler, and T. Pfau, J. Phys. B: At. Mol. Opt. Phys. **45**, 113001 (2012).

[36] M. D. Lukin, M. Fleischhauer, R. Cote, L. M. Duan, D. Jaksch, J. I. Cirac, and P. Zoller, Phys. Rev. Lett. **87**, 037901 (2001).

[37] E. Urban, T. A. Johnson, T. Henage, L. Isenhower, D. Yavuz, T. Walker, and M. Saffman, Nat. Phys. **5**, 110 (2009).

[38] C. Ates, T. Pohl, T. Pattard, and J. M. Rost, Phys. Rev. A **76**, 013413 (2007).

[39] G. Abumwis and S. Wüster, Phys. Rev. A **98**, 043606 (2018).

[40] The lifetime of N Rydberg atoms $\tau_{n,l}$ at zero temperature can be estimated by $\tau_{n,l} = \tau_0^{(l)} n^3/N$, where $\tau_0^{(l)}$ is the lifetime of a single Rydberg atom. For $n = 80$, we have $\tau_0^{(l)} \approx 0.058\ \mu$s from [43], hence for $N = 6$, $\tau_0^{(l)} \approx 50\ \mu$s.

[41] J. Lampen, H. Nguyen, L. Li, P. R. Berman, and A. Kuzmich, Phys. Rev. A **98**, 033411 (2018).

[42] G. Günter, H. Schempp, M. Robert-de-Saint-Vincent, V. Gavryusev, S. Helmrich, C. S. Hofmann, S. Whitlock, and M. Weidemüller, Science **342**, 954 (2013).

[43] I. I. Beterov, I. I. Ryabtsev, D. B. Tretyakov, and V. M. Entin, Phys. Rev. A **79**, 052504 (2009).